ELSEVIER

Catalysis Today 67 (2001) 189–203

CATALYSIS TODAY

www.elsevier.com/locate/cattod

Analysis of intermediate product yield in distributed-feed nonisothermal tubular membrane reactors

Anthony G. Dixon*

Department of Chemical Engineering, Worcester Polytechnic Institute, Worcester, MA 01609, USA

Abstract

A comparative study of yield to intermediate products obtained from the distributed-feed membrane reactor (MR) and the conventional cooled-tube plug-flow reactor (PFR) is presented. The nonisothermal, nonadiabatic one-dimensional pseudo-homogeneous reactor model was used. The analysis is presented in terms of the usual dimensionless groups (Damköhler number (*Da*), heat of reaction parameter, Stanton number (*St*), etc.) and delineates regions of parameter space where the membrane reactor gives improved yield with no higher maximum temperature. Optimal conditions for the PFR usually lie on or close to the boundaries between either pseudo-adiabatic operation (PAO) or hot-spot operation (HSO), and runaway operation.

Results show that when compared under optimal operating conditions and at the same catalyst volume, reactant feed rate, temperature and pressure, the membrane reactor performance is better than that of the PFR only over restricted regions of parameter space. In general, distributed feed is preferred at higher *Da*, and under conditions of high heat release or lower cooling rates. The distributed-feed reactor performance can be enhanced by a mixed-feed strategy, or by slightly increased inlet temperature.

Keywords: Membrane reactor; Packed-bed inert membrane reactor; Intermediate product yield; Nonisothermal membrane reactor

1. Introduction

There are many possible uses of membrane reactors (MR) to combine reaction and separation within a single processing unit. Such uses include product removal, distributed feed of a reactant and separated feed of two reactants, to name only some of the most studied. Much recent work has focused on the realistic assessment of future opportunities for membrane reactors [1], on the types of membrane reactor materials that are needed [2], and on problems and technical hurdles that must be overcome for industrial application of membrane reactors to become a reality [3]. Some niche areas where membrane reactors can make a unique contribution have been identified [4]. One of these is in the control of tubular reactor temperature profiles by distributed feed of a reactant through the reactor tube wall.

Membrane reactors can be used for reactions in which the yield of an intermediate product is of interest. A typical reaction scheme is of the consecutive-parallel type:

$$A + B \rightarrow R$$

$$A + R \rightarrow P + Q$$

where the reactions are parallel with respect to reactant A, and consecutive with respect to R. Many catalytic reactions of commercial importance have this structure, such as hydrocarbon partial oxidations,

* Tel.: +1-508-831-5350; fax: +1-508-831-5853.
E-mail address: agdixon@wpi.edu (A.G. Dixon).

0920-5861/01/$ – see front matter
PII: S0920-5861(01)00287-5

Nomenclature

B	heat-of-reaction parameter $(-\Delta\tilde{H}_1/\tilde{c}_{\mathrm{fS}}T_0)y^{\mathrm{S}}_{\mathrm{B}_0}\gamma$
$\tilde{c}_{\mathrm{fS}}$	average molar specific heat of shell side (kJ kg mol^{-1} K^{-1})
$\tilde{c}_{\mathrm{fT}}$	average molar specific heat of tube side (kJ kg mol^{-1} K^{-1})
$\tilde{c}_{\mathrm{p},i}$	heat capacity of species i (kJ kg mol^{-1} K^{-1})
Da	Damköhler number $(\pi(R_3^2 - R_2^2)L\rho_{\mathrm{B}}r_{\mathrm{ref}})/F_0$
E_j	activation energy for reaction j (kJ kg mol^{-1})
F_i	shell-side molar flow rate of species i (kg mol s^{-1})
F_{i_0}	shell-side inlet molar flow rate of species i (kg mol s^{-1})
F_i^*	dimensionless shell-side flow rate of species i, F_i/F_0
F_0	shell-side total molar flow rate (kg mol s^{-1})
ΔH_j	heat of reaction of reaction j (kJ kg mol^{-1})
k_{i_0}	pre-exponential reaction rate constant for reaction i
K	ratio of reaction rates $(k_{20}/k_{10})\,\mathrm{e}^{\gamma(1-\mu)}\,(P^{\mathrm{S}})^{n_2+n_{\mathrm{R}}-n_1-n_{\mathrm{B}}}$
L	reactor length (m)
n_{B}	kinetic order of species B in reaction 1
n_{R}	kinetic order of species R in reaction R
n_1	kinetic order of species A in reaction 1
n_2	kinetic order of species A in reaction 2
$N_{\mathrm{A,ref}}$	reference molar transmembrane flux, defined in Eq. (12) (kg mol m^{-2} s^{-1})
N_i	molar transmembrane flux of species i (kg mol m^{-2} s^{-1})
N_i^*	dimensionless molar transmembrane flux of species i, $N_i/N_{\mathrm{A,ref}}$
p_α	partial pressure on shell side of species α (kPa)
P^{S}	shell-side pressure (kPa)
P^{T}	tube-side pressure (kPa)
Pe	Peclet number, $F_0/(2\pi R_1 L N_{\mathrm{A,ref}})$
Q_i	tube-side molar flow rate of species i (kg mol s^{-1})
Q_{i_0}	tube-side inlet flow rate of species i (kg mol s^{-1})
Q_i^*	dimensionless tube-side flow rate of species i, Q_i/Q_0
Q_0	tube-side total molar flow rate (kg mol s^{-1})
r_j	reaction rate of reaction j (kg mol kg^{-1} s^{-1})
r_j^*	dimensionless reaction rate, r_j^*/r_{ref}
r_{ref}	reference reaction rate, defined in Eq. (11) (kg mol kg^{-1} s^{-1})
R_{g}	gas constant (kg m^2 s^{-2} kg mol^{-1} K^{-1})
R_1	inner membrane radius (m)
R_2	outer membrane radius (m)
R_3	inner shell radius (m)
S	ratio of total tube/shell-side flow rates, Q_0/F_0
St	Stanton number $(2\pi R_3 L U_3)/(F_0\tilde{c}_{\mathrm{fS}})$
T	reactor temperature (K)
T_{in}	inlet reactor temperature (K)
T_0	ambient (coolant) temperature (K)
U_{A}	permeability of species A through the membrane (kg mol m^{-1} s^{-1} kPa^{-1})
U_i	overall heat transfer coefficient, based on area at R_i (kW m^{-2} K^{-1})
x	dimensionless reactor length, z/L
y_{i_0}	inlet mole fraction of species i
y_α	mole fraction of species α
z	reactor length coordinate (m)

Greek symbols

α_{ij}	stoichiometric coefficient of species i in reaction j
δ	ratio of heat transfer rates, U_1R_1/U_3R_3
γ	dimensionless activation energy, $E/R_{\mathrm{g}}T_0$
λ	heat-of-reaction ratio, $\Delta H_2/\Delta H_1$
μ	activation energy ratio, E_2/E_1
θ	dimensionless reactor temperature $(T - T_0)\gamma/T_0$
ρ_{B}	bulk density of catalytic bed in shell side (kg m^{-3})

Subscripts

0	ambient conditions
α	species α, denoting A, B, or R

Superscripts

S	shell side (reaction side)
T	tube side (distributed reactant side)

where A represents oxygen, B represents a hydrocarbon, R the desired partial oxidation product, and P and Q the undesired total oxidation products (CO_2 and H_2O).

Reyes et al. have demonstrated, under isothermal conditions, that there can be a selectivity advantage to using an inert membrane reactor (IMR) to distribute a reactant, compared to the conventional co-feed mode of operation [5,6]. For favorable kinetics (the partial pressure of the distributed reactant appears to a lower order in the desired reaction rate expression than in the reaction rate expressions for the undesired reactions), the selectivity to intermediate products is better in the membrane reactor. One potential disadvantage is the fact that the lower average partial pressures of the distributed reactant (oxygen) lead to lower reaction rates in the membrane reactor. Thus, the gain in yield obtained in a membrane reactor due to increased selectivity may be offset (or more) by a decrease in conversion. In some instances, a prohibitively larger reactor volume may be required before the membrane reactor out-performs the tubular reactor, such as for the oxidative coupling of methane [5–7]. Harold and coworkers have demonstrated similar results for a catalytic membrane reactor (CMR) in which reactants A and B are segregated to opposite sides of a reactive membrane for the case of partial oxidation of ethylene to acetaldehyde [8,9]. For the oxidative dehydrogenation of ethane to ethylene, the experimental studies of Tonkovich et al. [10] showed the membrane reactor to out-perform a packed-bed inert membrane reactor (PBMR) under low feed-ratio conditions. For some reaction systems, such as ethylene epoxidation, uncertainty in the reaction kinetics make it unclear which reactant should be distributed. This was resolved experimentally in favor of distributing the ethylene [11]. Recent work on butane oxidation to maleic anhydride has suggested the use of a split-feed strategy to avoid oxygen starvation for the catalyst located near the reactor entrance [12].

The majority of studies have assumed isothermal conditions, as these are most often used in laboratory experimentation. Early studies considered nonisothermal conditions in specific dehydrogenation reactions [13,14], while Mohan and Govind provided a general analysis of a single reversible reaction in a PBMR [15]. Model equations for the nonisothermal case for both a PBMR and a CMR were given by Tsotsis et al. [16]. More recently, Koukou et al. [17] have simulated a PBMR using a two-dimensional model that included radial and axial dispersion, and have illustrated some important features of nonisothermal membrane reactor modeling.

A nonisothermal analysis of some product removal and reactant distribution applications using dense oxygen-conducting perovskite membranes in a PBMR was made by Dixon et al. [18], who showed that for *o*-xylene oxidation, a membrane reactor could not achieve the same yields to phthalic anhydride as a packed-bed reactor of the same volume, due to lower reaction rates, although the hot-spots were reduced in magnitude. Tsai et al. [19] analyzed the nonisothermal CMR for the partial oxidation of methane to syngas, and also showed lower hot-spot temperatures in the membrane reactor. Studies of a CMR to increase yield to intermediate products have been extended to nonisothermal conditions by Golman et al. [20] and Harold and Lee [21]. Saracco and Specchia [22] have analyzed steady-state multiplicity in a cooled, segregated-feed CMR for the catalytic combustion of propane. Good agreement between experiments and a nonisothermal model was achieved.

Experimental studies have been performed that have demonstrated the concept of safer operation and reduced hot-spot temperatures for VOC combustion [23] and for the oxidative dehydrogenation of butane [24] and ethane [10,25]. These studies have emphasized the avoidance of flammability limitations and the ability of the membrane reactor to operate under conditions that would lead to temperature runaway for a plug-flow reactor.

The PBMR has often been compared to the classical plug-flow or fixed-bed reactor (PFR) as a measure of its performance. The proper way to do this, short of a complete economic analysis, is not obvious. Lund and coworkers have considered the question at length, for membrane reactors used for the removal of intermediate products from partial oxidations [26,27], and for yield increases in reversible dehydrogenation reactions [28,29]. Their analysis in terms of standard dimensionless groups, delineated regions of parameter space where the membrane reactor could compete with the plug-flow reactor on the basis of yield alone. The limiting case of fast dehydrogenation reactions has been studied in general terms [30], as has been the case of isomerization reactions [31]. Boudart [32] has

suggested the use of an order-of-magnitude analysis to screen proposed membrane reactors for practicality under industrial conditions before proceeding with extended studies. A general analysis of isothermal reactant distribution reactors has been provided by Lu et al. [33].

The present modeling study focuses on the use of reactant distribution in MR to control temperature rise and to improve yield to intermediate products. To date, there have been no studies that attempt to determine general conditions under which the non-isothermal distributed-feed membrane reactor may be expected to out-perform a plug-flow reactor, from the viewpoint of both yield and thermal behavior. In this initial work, we considered a simple model representation of both reactors and optimized the operating conditions for the PFR with respect to feed of reactant A. The MR was then constrained to use the same catalyst volume as the PFR, with the same feed of hydrocarbon (B), and the range of membrane permeability to A was determined that allowed an increase in yield with no worse temperature rise in the MR. Regions where the MR out-performed the optimized PFR appeared in parameter space at higher space-times and for larger heat release or lower cooling rates.

2. Mathematical model

The MR considered here could be either a tube-and-shell IMR or PBMR, as depicted schematically in Fig. 1. The membrane tube was enclosed in a non-permeable outer shell, through which energy could be transferred to an external cooling or heating medium. Reactant B was fed to the shell or reaction side and reactant A to the tube side. The shell side could be packed with catalyst for the case of heterogeneous catalysis. Either or both reactants could be diluted with an inert carrier. Heat transfer also took place between the tube and shell sides. For the PFR, no transfer of species across the membrane tube was permitted and both reactants were co-fed to the shell side.

The model equations were derived on the basis of the following assumptions.

1. The reactor configuration was a one-dimensional tubular reactor with no axial dispersion. Radial concentration and temperature gradients were neglected on both the tube and shell sides. There was no gas film resistance to heat or mass transfer at the membrane walls.
2. The reactor was under constant pressure conditions, i.e. pressure drop was neglected on both the shell and tube sides.
3. The reactions were of the consecutive-parallel type discussed above, irreversible and subject to kinetic control. Reaction took place on the shell side only.
4. The membrane was permeable only to species A at a rate proportional to the difference in partial pressures of A across the membrane.
5. The reaction kinetics and reaction orders in the reactant concentrations were constant over the entire range of conditions simulated. Under reduced reactant concentrations, reaction orders can change or catalysts deactivate, but these effects were not included here.

The material balance on the shell (reaction) side for species i led to

$$\frac{\mathrm{d}F_i}{\mathrm{d}z} = \pi(R_3^2 - R_2^2)\rho_{\mathrm{B}}\sum_{j=1}^{NR}\alpha_{ij}r_j + 2\pi R_1 N_i \tag{1}$$

$$F_i(z=0) = F_{i_0} \tag{2}$$

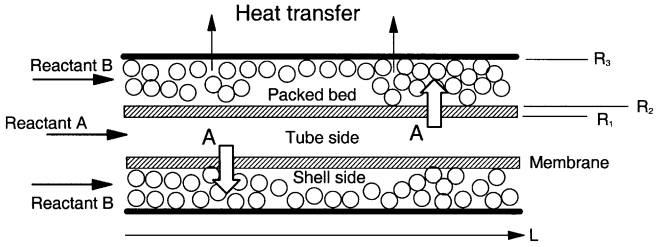

Fig. 1. Schematic of tube-and-shell membrane reactor.

and the material balance on the tube (distributed feed) side gave

$$\frac{\mathrm{d}Q_i}{\mathrm{d}z} = -2\pi R_1 N_i \tag{3}$$

$$Q_i(z=0) = Q_{i_0} \tag{4}$$

The reaction rates followed power-law kinetics as follows:

$$r_1 = k_{10}\,\mathrm{e}^{-E_1/(R_\mathrm{g}T^\mathrm{S})}\,p_\mathrm{A}^{n_1}\,p_\mathrm{B}^{n_\mathrm{B}} \tag{5}$$

$$r_2 = k_{20}\,\mathrm{e}^{-E_2/(R_\mathrm{g}T^\mathrm{S})}\,p_\mathrm{A}^{n_2}\,p_\mathrm{R}^{n_\mathrm{R}} \tag{6}$$

The energy balance for the shell side yielded

$$\sum_{i=1}^{NS} F_i \tilde{c}_{p_i}\,\frac{\mathrm{d}T^\mathrm{S}}{\mathrm{d}z} = 2\pi R_1 U_1 (T^\mathrm{T} - T^\mathrm{S}) + 2\pi R_3 U_3 (T_0 - T^\mathrm{S}) + \pi (R_3^2 - R_2^2)\rho_\mathrm{B} \sum_{j=1}^{NR} (-\Delta H_j) r_j \tag{7}$$

$$T^\mathrm{S}(z=0) = T_\mathrm{in} \tag{8}$$

and the energy balance on the tube side gave

$$\sum_{i=1}^{NS} Q_i \tilde{c}_{p_i}\,\frac{\mathrm{d}T^\mathrm{T}}{\mathrm{d}z} = 2\pi R_1 U_1 (T^\mathrm{S} - T^\mathrm{T}) \tag{9}$$

$$T^\mathrm{T}(z=0) = T_\mathrm{in} \tag{10}$$

For the PFR, the terms involving the permeation fluxes N_i were omitted from the material balances.

The model variables were made dimensionless with respect to total flow rate to the shell (reaction) side F_0, reactor length L, reference temperature T_0, a reference reaction rate defined with total shell-side pressure in reaction r_1:

$$r_\mathrm{ref} = k_{10}\,\mathrm{e}^{-E_1/(R_\mathrm{g}T_0)}\,(P^\mathrm{S})^{n_1+n_\mathrm{B}} \tag{11}$$

and a reference permeation rate based on air on one side and zero partial pressure of A on the other side of the membrane:

$$N_\mathrm{A,ref} = \frac{U_\mathrm{A}}{R_1 \ln(R_2/R_1)}\,p_{\mathrm{A}_0}^\mathrm{T} \tag{12}$$

The model was further simplified by the use of a constant molal heat capacity for both tube and shell sides, with average specific heats $\tilde{c}_\mathrm{fS}$ and $\tilde{c}_\mathrm{fT}$. Changing to dimensionless variables and introducing appropriate dimensionless parameters then yielded

$$\frac{\mathrm{d}F_i^*}{\mathrm{d}x} = Da\left[(\alpha_{i_1}\,\mathrm{e}^{\theta^\mathrm{S}/(1+\theta^\mathrm{S}/\gamma)}\,y_\mathrm{A}^{n_1} y_\mathrm{B}^{n_\mathrm{B}} + \alpha_{i_2} K\,\mathrm{e}^{\mu\theta^\mathrm{S}/(1+\theta^\mathrm{S}/\gamma)}\,y_\mathrm{A}^{n_2} y_\mathrm{R}^{n_\mathrm{R}}) + \frac{N_i^*}{DaPe}\right] \tag{13}$$

$$\frac{\mathrm{d}Q_i^*}{\mathrm{d}x} = -\frac{Da}{DaPe} N_i^* \tag{14}$$

$$\frac{\mathrm{d}\theta^\mathrm{S}}{\mathrm{d}x} = Da\left[\frac{St}{Da}(-\theta^\mathrm{S}) + \frac{St}{Da}\delta(\theta^\mathrm{T} - \theta^\mathrm{S}) + \frac{B}{y_{\mathrm{B}_0}^\mathrm{S}}(\mathrm{e}^{\theta^\mathrm{S}/(1+\theta^\mathrm{S}/\gamma)}\,y_\mathrm{A}^{n_1} y_\mathrm{B}^{n_\mathrm{B}} + \lambda K\,\mathrm{e}^{\mu\theta^\mathrm{S}/(1+\theta^\mathrm{S}/\gamma)}\,y_\mathrm{A}^{n_2} y_\mathrm{R}^{n_\mathrm{R}})\right] \tag{15}$$

$$\frac{\mathrm{d}\theta^\mathrm{T}}{\mathrm{d}x} = Da\left(\frac{St}{Da}\delta(\theta^\mathrm{S} - \theta^\mathrm{T})\frac{\tilde{c}_\mathrm{fS}}{\tilde{c}_\mathrm{fT}}\frac{1}{S}\right) \tag{16}$$

The initial conditions were

$$F_i^*(x=0) = y_{i_0}^\mathrm{S} \tag{17}$$

$$Q_i^*(x=0) = y_{i_0}^\mathrm{T} S \tag{18}$$

$$\theta^\mathrm{S}(x=0) = \theta_\mathrm{in}^\mathrm{S} \tag{19}$$

$$\theta^\mathrm{T}(x=0) = \theta_\mathrm{in}^\mathrm{T} \tag{20}$$

Again, the equations for the PFR could be recovered in the limit $Pe \to \infty$.

These equations formed a set of nonlinear initial-value ODEs, which were solved using a standard algorithm with Gear's implicit backward difference formulas and a divided difference approximation to the Jacobian. Under some conditions, the equations were quite stiff. All optimizations were performed by brute-force one-dimensional search.

The conversion of reactant B and selectivity to product R were calculated from

$$\chi = 1 - \frac{F_\mathrm{B}}{F_{\mathrm{B}_0}}, \qquad S_\mathrm{R} = \frac{F_\mathrm{R}}{F_{\mathrm{B}_0} - F_\mathrm{B}} \tag{21}$$

and the yield to R was given by $Y = \chi S_\mathrm{R}$. The amounts of species A consumed in both the PFR and

the membrane reactor were calculated, and the ratio given by

$$\frac{A_{MR}}{A_{PFR}} = \frac{[y^S_{A_0} + S(y^T_{A_0} - y^T_A(1))]_{MR}}{(y^S_{A_0})_{PFR}} \quad (22)$$

All calculations presented in Section 3 were made using a base set of parameter values, unless otherwise indicated. Those values were $Da = 1$, $B = 14$, $St/Da = 5$, $\gamma = 20$, $\mu = 1.75$, $\lambda = 2.0$, $K = 0.5$, $\delta = 0.25$, $S = 1000$, $y_{A_0} = y_{B_0}$, $n_1 = 0.5$, $n_2 = n_B = n_R = 1.0$, and all stoichiometric coefficients were unity. These values somewhat loosely reflected the typical range for partial oxidation reactions, given by Varma et al. [34] and Harold and Lee [21]. The ratio of tube-to-shell total flow rates, S, was chosen to be large enough to avoid problems of reactant depletion. It was preferred to work in terms of the groups St/Da and $DaPe$, rather than St and Pe directly, as this choice eliminated the reactor length and flow rate from St/Da and $DaPe$, so that Da was the only parameter reflecting reactor residence time.

3. Results and discussion

From the dimensionless Eqs. (13)–(16) and their initial conditions (17–20), there were clearly too many parameters for a complete evaluation of the model parameter space. The point of view taken was, therefore, that of reactor design for a specified reaction at given total pressures P^S (and P^T for the MR) and coolant temperature T_0. This then enabled γ, K, μ, and λ to be removed as candidates for optimization. The reaction orders and stoichiometry were fixed, and δ and S were regarded as being of lesser importance. The study focused on the behavior of the reactors with respect to Da, B (essentially y_{B_0} since $\Delta\tilde{H}_1/\tilde{c}_{fS}T_0$ was fixed), St/Da and the feed ratio ϕ_r.

The behavior of the PFR for series and parallel reaction schemes has been extensively investigated, most recently by Varma et al. [34]. They classified reactor operation into three regimes: pseudo-adiabatic operation (PAO) in which the reactor temperature increased monotonically from the inlet to the outlet of the reactor; hot-spot operation (HSO) in which there

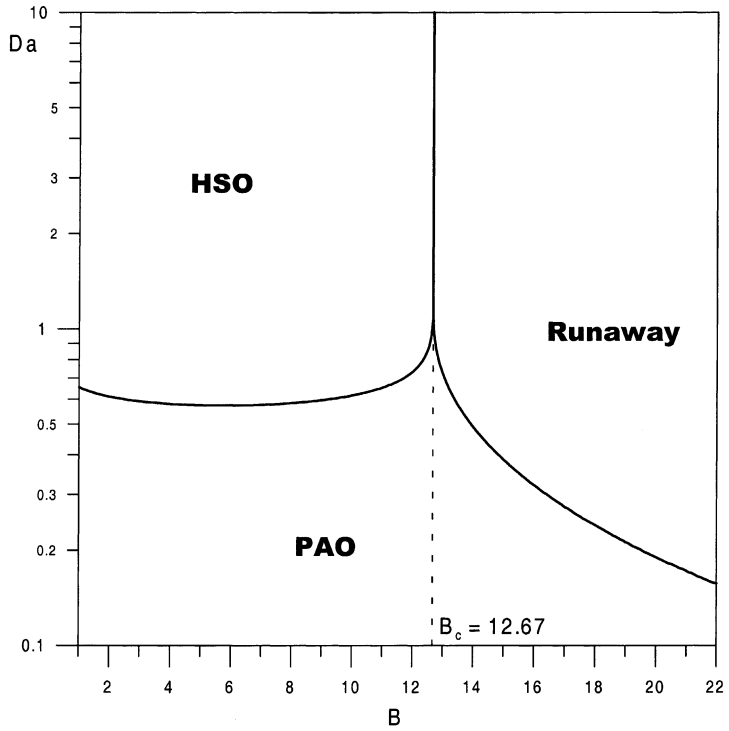

Fig. 2. Behavior regions for the PFR in the Da–B parameter plane for base-case conditions.

was a maximum in the temperature; runaway, corresponding to the region of parametric sensitivity and in which temperature increased dramatically. They presented diagrams of the *St–Da* and *Da–B* parameter planes with the three regions of operation delineated for each type of reaction scheme in the PFR. They did not investigate the consecutive-parallel scheme considered here, although it might be expected to show similar characteristics.

3.1. Behavior and optimal yield in the PFR

The model equations were integrated over ranges of values of B and Da and for the base-case values of the other parameters given above. For each B, Da was increased from a very low value, where PAO operation was assured, until a temperature maximum was observed. The last Da value before the appearance of the maximum gave the point on the PAO/HSO or PAO/runaway boundary. The results for the base case are presented in the *Da–B* plane in Fig. 2, and followed the same qualitative trends as seen by Varma et al. [34]. At lower B, increasing Da caused a transition from PAO to HSO operation. At higher B, increasing Da caused a transition from PAO to runaway operation. A critical value of the heat release parameter, $B = B_c$, separated these two behaviors. Above B_c, the heat release was high enough to cause the reactor to run away, unless the development of the temperature was limited by the short reactor length, as was the case for smaller Da. As B increased, the reactor length needed to accommodate runaway decreased. The HSO/runaway boundary at $B = B_c$ was obtained from the peak in the PAO boundary, and verified a posteriori by solving the model for B values above and below B_c. Note that changing B with constant $\Delta\tilde{H}_1/\tilde{c}_{fS}T_0$ was equivalent to changing the inlet mole fraction y_{B_0} in the initial conditions of the model.

The overall pattern of behavior for the PFR remained the same for other values of the parameters. A typical example, showing the effect of varying the feed ratio ϕ_r, is shown in Fig. 3. As ϕ_r was increased,

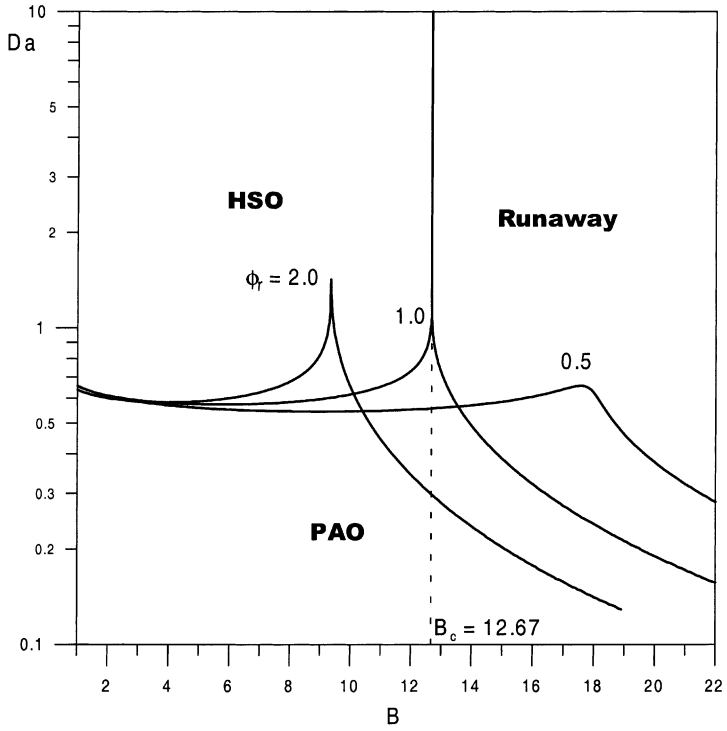

Fig. 3. Behavior regions for the PFR in the *Da–B* parameter plane for various values of ϕ_r.

the runaway region increased in size and B_c moved to lower B values, reflecting the higher reaction rates available with higher reactant feeds. For milder conditions with lower heat release, the peak in the PAO boundary became more diffuse, and the value of B_c was harder to determine. Parametric sensitivity analysis [34] would be needed for more precise location of B_c. Similar results were obtained with the other parameters, with *St*/*Da* and n_1 especially having a strong influence on the operation regions, while γ, K, μ, and λ had relatively minor effects.

The parameters that were considered to be adjustable to obtain optimal yield of R were *Da* (reactor length), *St*/*Da* (heat-removal rate) and ϕ_r (A-to-B feed ratio). In this study, only single-variable optimizations were considered, with other parameters held at their base-case values. The feed of reactant B was considered to be specified at a given value for each case.

The PFR was first optimized with respect to *Da*. Two regions of distinct behavior were observed. For $B > B_c$, the optimal *Da* values coincided with the PAO boundary. Under these conditions, the yield was limited by conversion, which was in turn limited by reactor length. Heat effects were strong enough to cause runaway, so the optimal value of *Da* was as large as possible to maximize conversion, but short of the loss of selectivity associated with runaway. These operating conditions would, of course, be impractical in a real reactor, but may serve as a benchmark for comparison to the membrane reactor. For $B < B_c$, heat effects would not cause runaway, and yield increased with reactor length towards an asymptotic value. There was therefore no optimal value of *Da* for this region.

The PFR was next optimized with respect to ϕ_r for each value of *Da* over a reasonable range. Several values of B and of *St*/*Da* were examined, as shown in Figs. 4 and 5 in the ϕ_r–*Da* plane. The maximum value of ϕ_r was constrained by the value of y_{B_0}, resulting in the horizontal segments of ϕ_r^{opt} at very low *Da*. As *Da* was increased, ϕ_r^{opt} decreased following the PAO–runaway boundary, with some deviation for $B = 7$. When the critical value of ϕ_r for runaway was

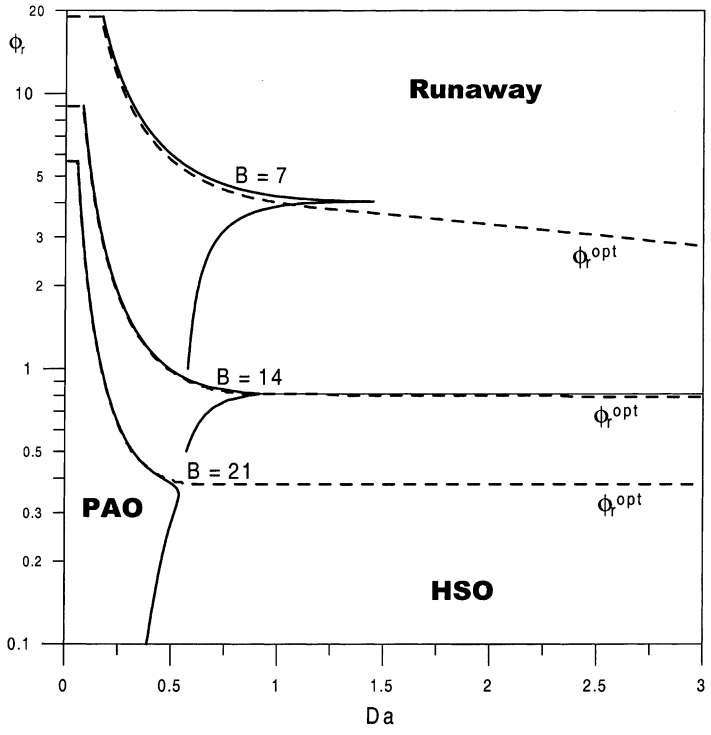

Fig. 4. Optimal ϕ_r operation curves for maximum PFR yield to intermediate product R in the ϕ_r–*Da* parameter plane for various values of heat-of-reaction parameter B.

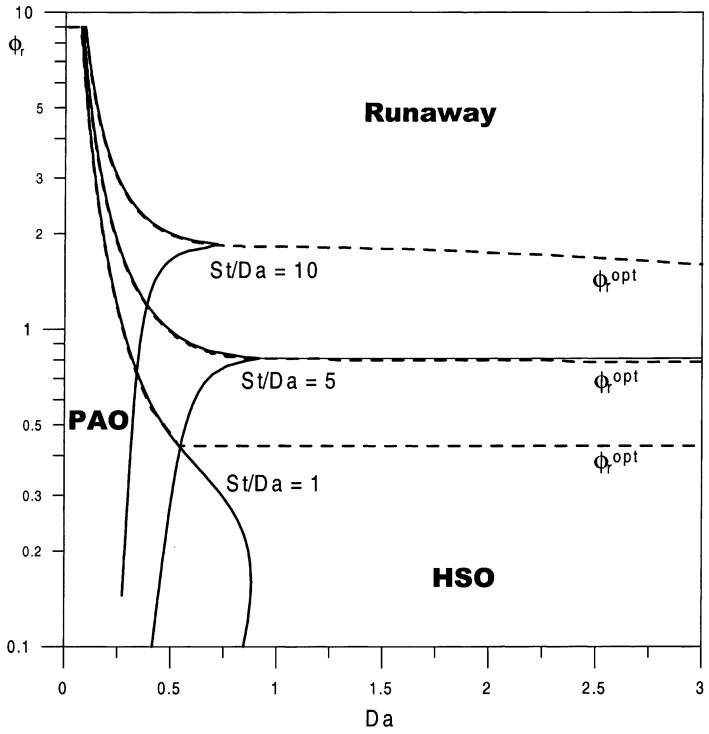

Fig. 5. Optimal ϕ_r operation curves for maximum PFR yield to intermediate product R in the ϕ_r–*Da* parameter plane for various values of heat-removal parameter *St*/*Da*.

passed, ϕ_r^{opt} continued to decrease but at a very low rate, broadly following the HSO–runaway boundary, or slightly into the HSO region. The interpretation of these optimal curves is that for a fixed reactor length (*Da*), conversion generally increased and selectivity decreased as ϕ_r increased. The effect of conversion was stronger, so yield was increased by operating with as high a ϕ_r as possible without runaway. For longer reactors, however, a point was reached where the decrease in selectivity outweighed the increase in conversion before runaway occurred, and so yield decreased and the optimum ϕ_r was found for values below the runaway limit. For two cases, it was not easy to identify the onset of runaway and the location of the HSO–runaway boundary was in doubt.

The PFR was finally optimized with respect to *St*/*Da* for a range of values of *Da*. The results were similar to those obtained for ϕ_r and will not be further discussed here. The ϕ_r^{opt} curves obtained above provide a benchmark of PFR performance with which to compare the MR.

3.2. Comparison of MR and PFR

The purpose of the comparisons presented here was to determine if a membrane reactor could perform better than a suitably optimized plug-flow reactor. If better performance was possible, it was desired to learn how much better could be achieved and over what range of membrane permeability, and for what ranges of reactor operation. To quantify better performance, two criteria were employed: (i) the yield of the MR to the valuable product R should be higher than in the PFR; (ii) the maximum temperature in the MR should not be higher than in the PFR.

The comparisons were made under the following conditions:

1. equal *Da*, i.e. equal reactor/catalyst volume and total reaction side flow rate F_0;
2. equal feed of reactant B, i.e. equal y_{B_0} or heat-of-reaction parameter *B*;
3. equal heat-removal rate *St*/*Da* (and δ, *S*, T_0).

All parameters pertaining to reactions such as kinetic orders, γ, K, μ, and λ were held the same, as were physical properties such as heat capacities. It was explicitly not required that each reactor use the same amount of reactant A. One advantage of a membrane reactor is to be able to run under more favorable conditions of temperature or reactant feed than is possible with the plug-flow reactor. For this study, reactant A was regarded as being inexpensive, and each reactor was allowed to make the best use of it that it could.

The procedure for determining when the MR performance was better is illustrated in Fig. 6. This is a plot of the ratio of MR yield to PFR yield, against the ratio of MR maximum temperature rise to PFR maximum temperature rise. The top-left quadrant is the region in which the membrane reactor satisfies the two performance criteria. For fixed values of B and Da, the MR model was solved for a series of decreasing values of $DaPe$, or increasing values of the parameter $1/Pe$, which is proportional to the permeability of A. This resulted in a trajectory in the membrane performance plane that started at low yield and temperature rise ratios, and in general both increased as the amount of A increased. Three types of trajectory are illustrated: for $B = 14$ and $Da = 1$, the MR temperature rise exceeded that of the PFR while the yield was still less, so no range of membrane permeability gave rise to an advantage; for $B = 14$ and $Da = 3$, the MR to PFR yield ratio exceeded unity for a range of permeabilities given by the interval $[DaPe_H, DaPe_L]$ as shown, before falling below unity again; for $B = 20$ and $Da = 6$, the MR to PFR yield ratio again exceeded unity for a range of permeabilities given by a different interval $[DaPe_H, DaPe_L]$, after which the MR to PFR temperature rise ratio exceeded unity.

The limiting values $DaPe_H$ and $DaPe_L$ obtained from each trajectory that passed through the upper-left quadrant of the reactor performance plane were converted using Da to the corresponding values Pe_H and Pe_L. Their reciprocals gave lower and upper limits, respectively, on the membrane permeability range over which the MR would have an advantage. These quantities are plotted in Figs. 7–10 to delineate the MR-favorable regions.

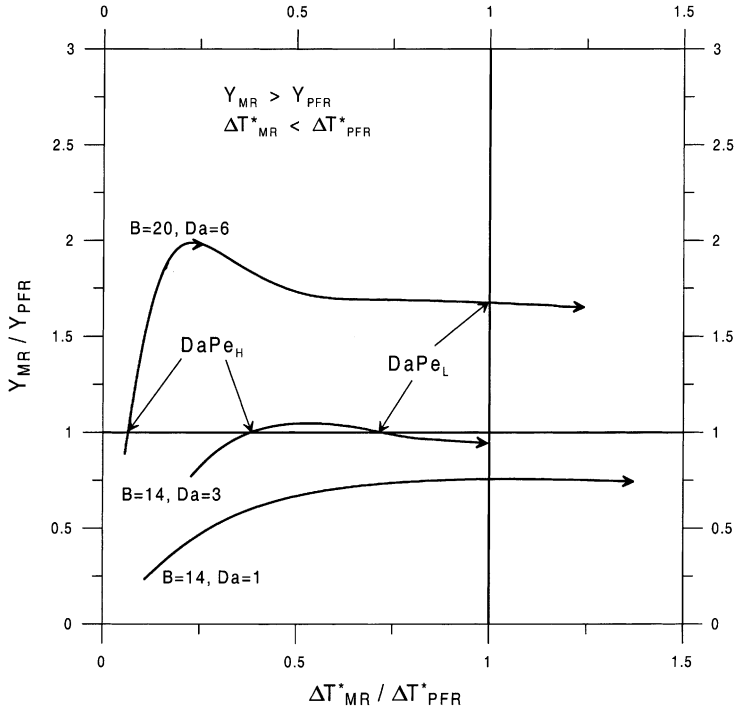

Fig. 6. *DaPe* trajectories for the membrane reactor in the plane of relative yield vs. relative temperature rise for various values of *Da*.

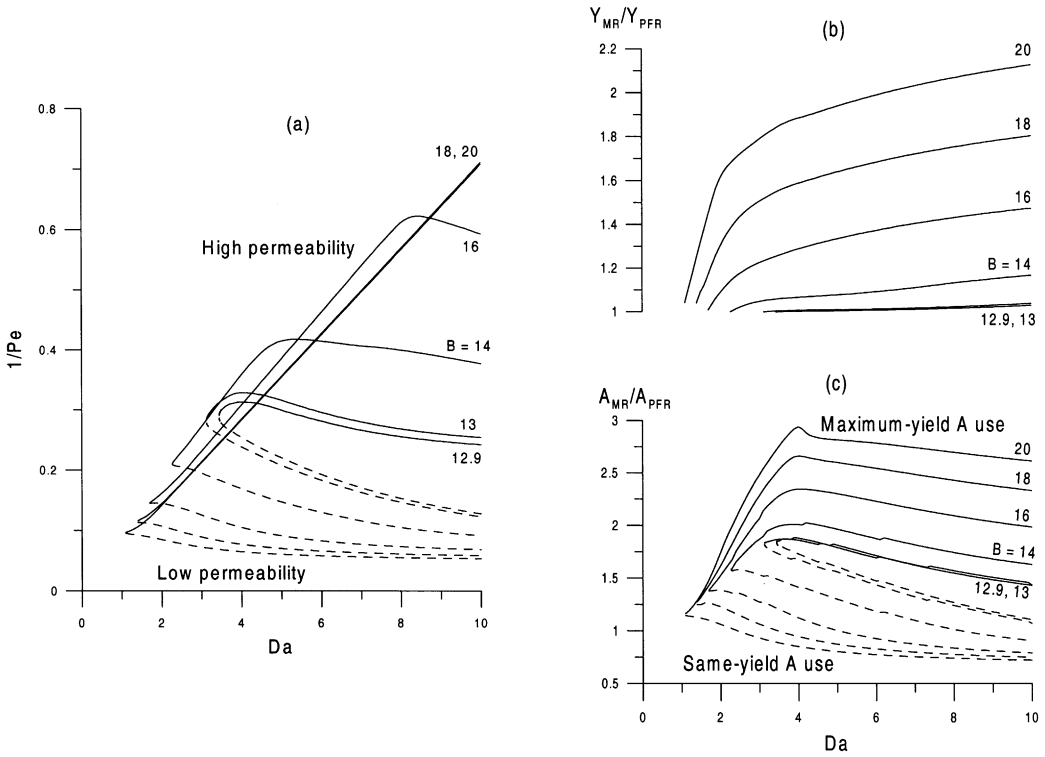

Fig. 7. Comparison of membrane reactor to ϕ_r-optimized PFR for various values of heat-of-reaction parameter B: (a) regions of improved yield in the $1/Pe$–Da plane; (b) maximum yield ratio for MR relative to PFR; (c) consumption of A in MR relative to PFR.

The MR was compared to the ϕ_r-optimal PFR over the range $0.1 \leq Da \leq 10$ and for several values of B, the other parameters being at their base-case values. For $B < 12.9$, no MR-favorable region existed; at higher values of B, the results are shown in Fig. 7. For each value of B, two curves are shown in Fig. 7a, the upper full one corresponding to the upper limit on membrane permeability and the lower dashed curve corresponding to the lower limit on membrane permeability. Below the lower limit, the conversion of the MR was too low for it to compete with the PFR due to the low supply of reactant A. Above the upper limit, the supply of reactant A was too high, leading to a loss in selectivity and giving yield below that of the PFR once more. As the heat-of-reaction parameter B increased, the MR-favorable region extended to lower values of Da, and over a wider range of $1/Pe$. In particular, the lower limit on permeability decreased with higher B, since the higher temperatures in the reactor allowed the conversion level to be maintained at lower levels of A.

The shape of the MR-favorable region was influenced by the competition between conversion and selectivity in a distributed-feed reactor for a consecutive-parallel reaction scheme, as Da and permeability $1/Pe$ were varied. For a fixed Da, increasing $1/Pe$ caused conversion to increase, rapidly at first and then more slowly. Selectivity decreased as $1/Pe$ increased, slowly at first and then more rapidly. Both effects were caused by higher levels of reactant A in the reactor which increased reaction rates, especially that of the nonselective reaction. The yield therefore passed through a maximum as $1/Pe$ increased. For a fixed $1/Pe$, increasing Da caused conversion to increase, also rapidly at first then more slowly, due to the increased reaction rate. Selectivity again decreased as Da increased, slowly at first then more rapidly. The reason for this was that at higher Da, the

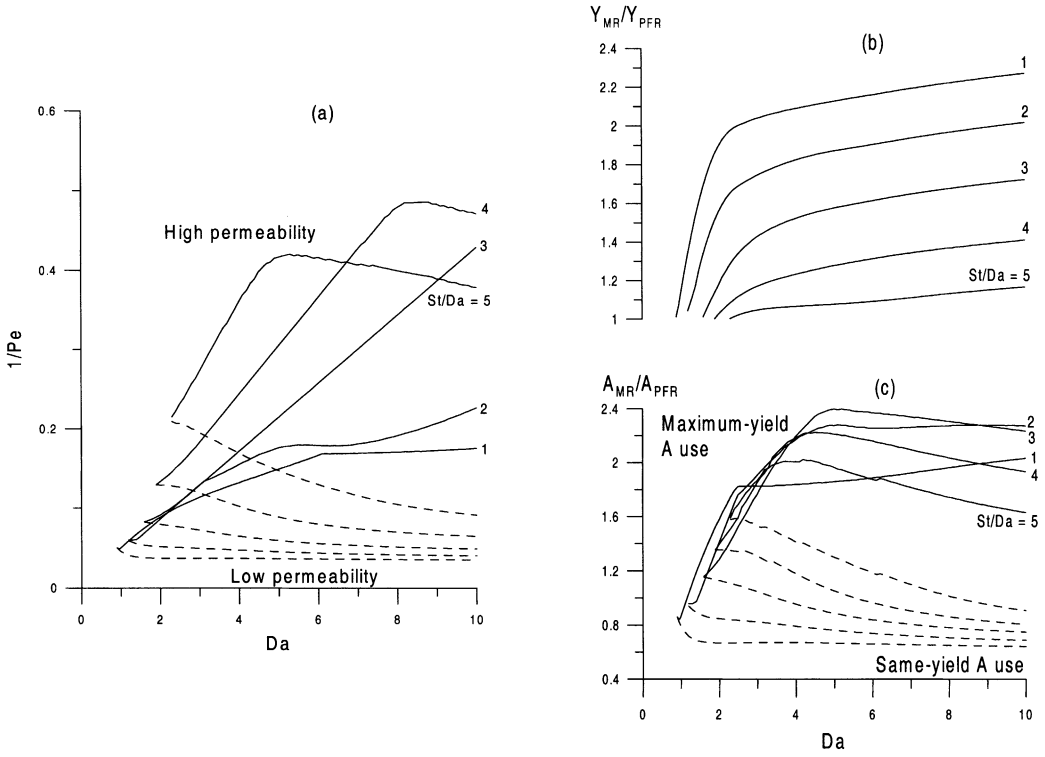

Fig. 8. Comparison of membrane reactor to ϕ_r-optimized PFR for various values of heat-removal parameter *St*/*Da*: (a) regions of improved yield in the 1/*Pe*–*Da* plane; (b) maximum yield ratio for MR relative to PFR; (c) consumption of A in MR relative to PFR.

selective reaction occurred further upstream, giving more opportunity for the product R to react downstream with the freshly fed reactant A. The yield passed through a maximum as *Da* increased.

The results of these effects were the following. At lower *Da*, for a given 1/*Pe*, if *Da* was increased then yield would increase above the level needed to match the PFR at the new *Da*. It was then possible to increase 1/*Pe* before decreasing yield to the PFR level. So at lower *Da*, the upper limit on 1/*Pe* increased. At higher *Da*, for a given 1/*Pe*, if *Da* was increased, the yield decreased due to loss of selectivity so that 1/*Pe* had to be kept the same or decreased to restore selectivity and maintain the yield at the PFR level. So at higher *Da*, the upper limit on 1/*Pe* slightly decreased. This explains why the upper permeability limit increased almost linearly with *Da*, then peaked and decreased slowly.

For a particular *B*, as *Da* increased the lower permeability limit decreased relatively slowly. For the lower limit, as *Da* increased the reaction rate increased, and conversion could be maintained high enough to match the PFR yield even at lower levels of reactant A.

Maximum yield was achieved in the MR at a *DaPe* value between the limits, and is shown as a ratio to PFR yield in Fig. 7b. The improvement in yield increased with *Da*, and also with *B*. So the membrane reactor could give significantly better yield than the plug-flow reactor for higher reaction rates, higher reactor volumes, and stronger heat effects. The improvement had a price, however, as is shown in Fig. 7c, which shows the ratio of reactant A usage in both reactors as defined in Eq. (22). The dashed curves show the ratio when the MR had the same yield as the PFR, and the full curves show the usage for the maximum MR yield. Clearly, the MR used much more reactant A to obtain the improved yield, and this use increased with *B*, and went through a maximum with *Da*. If the MR was restricted to the same amount of A as the PFR, there would be only extremely small regions where it could compete.

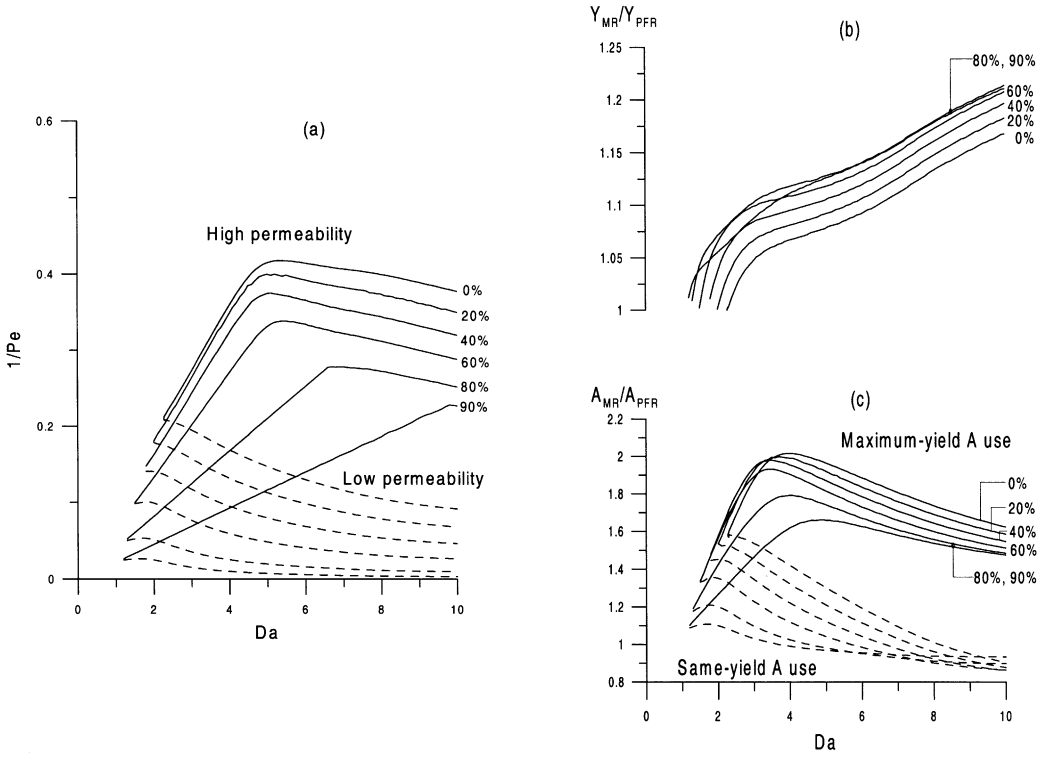

Fig. 9. Comparison of membrane reactor to ϕ_r-optimized PFR, effect of split feed of A: (a) regions of improved yield in the 1/*Pe*–*Da* plane; (b) maximum yield ratio for MR relative to PFR; (c) consumption of A in MR relative to PFR.

The MR was also compared to the ϕ_r-optimal PFR over the range $0.1 \leq Da \leq 10$ for $B = 14$, and several values of heat-removal parameter *St*/*Da*. For higher $St/Da > 5$, no MR-favorable region could be found. For lower values of *St*/*Da*, results are shown in Fig. 8, where $St/Da = 5$ was the base-case value. For $St/Da = 4$ or 3, the heat-removal rate was lower, and the MR-favorable region shifted to lower 1/*Pe* at moderate *Da*, extended slightly to lower *Da* and allowed higher A permeability at larger *Da* values. The lower limit also decreased. For $St/Da = 2$, the upper limit corresponded to higher ΔT in the MR than in the PFR and was parametrically sensitive. The shape of the curve depended in a complex way upon PFR behavior and on MR behavior close to runaway. For $St/Da = 1$, there was a sharp change in slope of the upper bound. For *Da* below this point, the limit on 1/*Pe* was reached when MR yield dropped below that of the PFR. For *Da* above this point, the limit on 1/*Pe* was reached when the ΔT_{MR} exceeded ΔT_{PFR}.

One drawback to feed distribution through a membrane is that the first part of the MR is poorly used, as there is no reactant A at the reactor entrance. The catalyst may also be adversely affected [12]. To improve MR performance, we can consider a split feed, where some of reactant A is fed to the shell side as well as distributing it from the tube side. Results are shown in Fig. 9 for the base case. For each *Da*, the PFR used an amount of reactant A corresponding to the previously determined ϕ_r^{opt}. The MR was simulated using the indicated percentages of the ϕ_r^{opt} for the PFR. Thus, 0% would correspond to the MR simulations presented in Fig. 7, and 100% would correspond to co-feeding the MR with the same amount of reactant A as the PFR.

The results in Fig. 9 show that as the percentage increased, the MR-favorable region moved to lower *Da* and lower 1/*Pe*. The widest range of permeability was at intermediate percentages. As percentage increased so did maximum yield up to 80%; for higher percentages, the yield could decrease at lower *Da*. Also, as

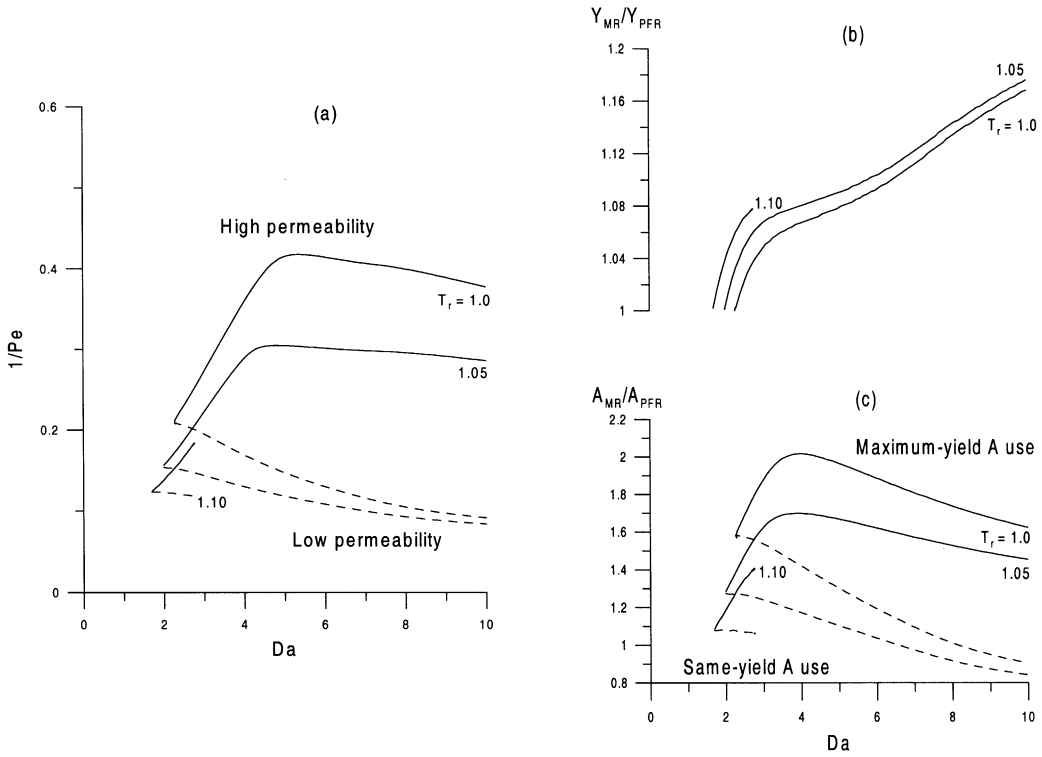

Fig. 10. Comparison of membrane reactor to ϕ_r-optimized PFR, effect of increased inlet temperature in membrane reactor: (a) regions of improved yield in the 1/*Pe*–*Da* plane; (b) maximum yield ratio for MR relative to PFR; (c) consumption of A in MR relative to PFR.

percentage increased, the total use of A decreased, so that the MR made more efficient use of A when a split-feed strategy was used. The trend changed for 80 and 90%, where more A was used than for 60%, so there appears to be an optimal level of co-feed for a membrane reactor.

An alternative method of increasing utilization of the reactor entrance region is to increase the inlet temperature. The rationale is that since heat release is more evenly distributed along the MR, it should be possible to sustain a higher inlet temperature without increasing the maximum temperature rise. Fig. 10 shows the results of this approach for the base case for different values of $T_r = T_{in}/T_0$ for the membrane reactor. For the PFR, $T_r = 1$ for all cases. As T_r increased from 1.0 to 1.1, the MR-favorable region decreased in size, but moved to lower *Da* and lower permeability. For $T_r > 1.10$, no region of advantage could be found. As T_r increased, the yield ratio increased and the use of A decreased.

The MR was also compared to the *Da*-optimal PFR over a range of $B > B_c$ and to the *St*/*Da*-optimal PFR over a range of *Da*, both for base-case values of the other parameters. In both cases, no range of membrane permeability could be found for which the MR had an advantage.

4. Conclusions

The yield to an intermediate product in a series–parallel reaction scheme has been compared for a plug-flow reactor and a distributed reactant feed membrane reactor. The reactors were simulated using simplified two-dimensional pseudo-homogeneous nonisothermal models as a first approach. The behavior and trends reported here should be interpreted taking into account the simplified nature of the models. More realistic modeling in future work is needed to confirm the results.

The behavior of a plug-flow reactor is conveniently represented in terms of the boundaries between three types of behaviors: pseudo-adiabatic operation, hot-spot operation, and runaway. Optimal operation of a PFR with respect to feed ratio, reactor length, or heat-removal rate leads to conditions on or close to runaway boundaries. These conditions provide a stiff benchmark for the membrane reactor for the criteria of improved yield and no worse temperature rise than the PFR.

Regions of membrane reactor advantage lie mainly at higher reactor lengths or reaction rates (higher *Da*). The regions are wider for more thermally challenging conditions, higher heat-reaction parameter *B* or lower heat-removal rate *St*/*Da*. The gain in yield also increases with *Da* and *B*, and significantly better yields can be obtained under some conditions. The membrane reactor uses considerably higher amounts of the distributed reactant A.

Under-utilization of the entrance region of the reactor can be improved by co-feeding some reactant A as well as distributing it. The membrane reactor uses less reactant A in total under this split-feed arrangement, and the membrane permeability requirement decreases. Similar results can be obtained by increasing the membrane reactor inlet temperature, but over more limited ranges of *Da*.

References

[1] J. Sanchez, T.T. Tsotsis, in: A.J. Burggraaf, L. Cot (Eds.), Fundamentals of Inorganic Membrane Science and Technology, Elsevier, Amsterdam, 1996, pp. 529–568.

[2] J. Coronas, J. Santamaría, Catal. Today 51 (1999) 377–389.

[3] G. Saracco, H.W.J.P. Neomagus, G.F. Versteeg, W.P.M. van Swaaij, Chem. Eng. Sci. 54 (1999) 1997–2017.

[4] A.G. Dixon, in: J.J. Spivey (Ed.), Specialist Periodical Reports: Catalysis, Vol. 14, Royal Society of Chemistry, London, 1999, pp. 40–92.

[5] S.C. Reyes, E. Iglesia, C.P. Kelkar, Chem. Eng. Sci. 48 (1993) 2643–2661.

[6] S.C. Reyes, C.P. Kelkar, E. Iglesia, Catal. Lett. 19 (1993) 167–180.

[7] Y. Lu, A.G. Dixon, W.R. Moser, Y.H. Ma, Ind. Eng. Chem. Res. 36 (1997) 559–567.

[8] M.P. Harold, V.T. Zaspalis, K. Keizer, A.J. Burggraaf, Chem. Eng. Sci. 48 (1993) 2705–2725.

[9] K. Keizer, V.T. Zaspalis, R.S.A. de Lange, M.P. Harold, A.J. Burggraaf, in: J.G. Crespo, K.W. Boddeker (Eds.), Membrane Processes in Separation and Purification, Kluwer Academic Publishers, Dordrecht, 1994, pp. 415–429.

[10] A.L.Y. Tonkovich, J.L. Zilka, D.M. Jimenez, G.L. Roberts, J.L. Cox, Chem. Eng. Sci. 51 (1996) 789–806.

[11] M.A. Peña, D.M. Carr, K.L. Yeung, A. Varma, Chem. Eng. Sci. 53 (1998) 3821–3834.

[12] R. Mallada, M. Menéndez, J. Santamaría, Catal. Today 56 (2000) 191–197.

[13] M. Oertel, J. Schmitz, W. Weirich, D. Jendryssek-Nermann, R. Schulten, Chem. Eng. Technol. 10 (1987) 248–255.

[14] K. Mohan, R. Govind, Ind. Eng. Chem. Res. 27 (1988) 2064–2070.

[15] K. Mohan, R. Govind, Sep. Sci. Technol. 23 (12/13) (1988) 1715–1733.

[16] T.T. Tsotsis, A.M. Champagnie, S.P. Vasileiadis, Z.D. Ziaka, R.G. Minet, Chem. Eng. Sci. 47 (1992) 2903–2908.

[17] M.K. Koukou, G. Chaloulou, N. Papayannakos, N.C. Markatos, Int. J. Heat Mass Transfer 40 (1997) 2407–2417.

[18] A.G. Dixon, Y.H. Ma, W.R. Moser, Ind. Eng. Chem. Res. 33 (1994) 3015–3024.

[19] C.-Y. Tsai, Y.H. Ma, W.R. Moser, A.G. Dixon, Chem. Eng. Commun. 134 (1995) 107–132.

[20] B. Golman, K. Shinohara, M. Kobayashi, J. Chem. Eng. Jpn. 30 (1997) 507–513.

[21] M.P. Harold, C. Lee, Chem. Eng. Sci. 52 (1997) 1923–1939.

[22] G. Saracco, V. Specchia, Chem. Eng. Sci. 55 (2000) 3979–3989.

[23] J. Coronas, M. Menéndez, J. Santamaría, J. Loss Prev. Process Ind. 8 (1995) 97–101.

[24] C. Téllez, M. Menéndez, J. Santamaría, AIChE J. 43 (1997) 777–784.

[25] F.A. Al-Sherehy, A.M. Adris, M.A. Soliman, R. Hughes, Chem. Eng. Sci. 53 (1998) 3965–3976.

[26] S. Agarwalla, C.R.F. Lund, J. Membr. Sci. 70 (1992) 129–141.

[27] L.A. Bernstein, C.R.F. Lund, J. Membr. Sci. 77 (1993) 155–164.

[28] C.M. Reo, L.A. Bernstein, C.R.F. Lund, AIChE J. 43 (1997) 495–504.

[29] C.M. Reo, L.A. Bernstein, C.R.F. Lund, Chem. Eng. Sci. 52 (1997) 3075–3083.

[30] M. Sheintuch, Ind. Eng. Chem. Res. 37 (1998) 807–814.

[31] D. Chmielewski, Z. Ziaka, V. Manousiouthakis, Chem. Eng. Sci. 54 (1999) 2979–2984.

[32] M. Boudart, CATTECH 12 (1997) 94.

[33] Y. Lu, A.G. Dixon, W.R. Moser, Y.H. Ma, Chem. Eng. Sci. 52 (1997) 1349–1363.

[34] A. Varma, M. Morbidelli, H. Wu, Parametric Sensitivity in Chemical Systems, Cambridge University Press, Cambridge, 1999.